POLITECNICO
MILANO 1863

SCUOLA DI INGEGNERIA INDUSTRIALE
E DELL'INFORMAZIONE

Executive Summary of the Thesis

Commissioning and performance evaluation of a Ge(nn0) Johansson crystal analyzer for lab-based X-ray spectroscopy

Laurea Magistrale in Engineering physics - Ingegneria fisica

Author: Farnaz Golpayegani

Advisor: Prof. Marco Moretti

Co-advisor: Dr. Roberto Sant

Academic year: 2025-2026

1. Introduction

X-ray Absorption Spectroscopy (XAS) probes the local electronic and atomic structure of materials through the energy-dependent absorption of X-rays [1] . In many applications, high energy resolution is required to resolve weak spectral features and subtle changes. While synchrotron beamlines provide excellent XAS capabilities, routine measurements are often limited by cost, limited access, and scheduling constraints.

Within the NEXT-GAME activity, Politecnico di Milano is developing a laboratory-based XAS spectrometer (LabXAS) to enable regular measurements in the Department of Chemistry and to reduce dependence on synchrotron facilities. My thesis work is part of this larger collaborative project and focuses on commissioning and quantitatively benchmarking Ge(nn0) bent-crystal analyzers. Key performance aspects are validated under controlled synchrotron conditions, including energy resolution (FWHM), reflectivity, and detector footprint, providing a reference baseline prior to full laboratory operation. In particular, I analyzed datasets collected at the synchrotron facility to quantify the crystal/analyzer performance.

2. Laboratory XAS Concept and Optical Geometry

A laboratory XAS spectrometer is a compact energy-selective system composed of an X-ray source, a bent-crystal analyzer, and a detector. The source delivers a polychromatic, generally non-collimated beam; the analyzer selects a narrow energy band via Bragg reflection; and the detector records the reflected intensity. Unlike synchrotron beamlines, where energy selection is typically set upstream by a double-crystal monochromator, in a laboratory spectrometer the analyzer itself defines the effective energy selection and thus directly affects the achievable energy resolution.

In the LabXAS developed at Politecnico di Milano, the source–analyzer–detector layout follows a Rowland-circle geometry to focus the selected energy onto the detector. The source is kept fixed (outside the vacuum chamber), while the analyzer and detector are inside the chamber and move/rotate in a coordinated way during energy scanning. Figure 1 shows the setup: (a) the instrument and (b) an interior view marking the source (S), analyzer (A), and detector (D).

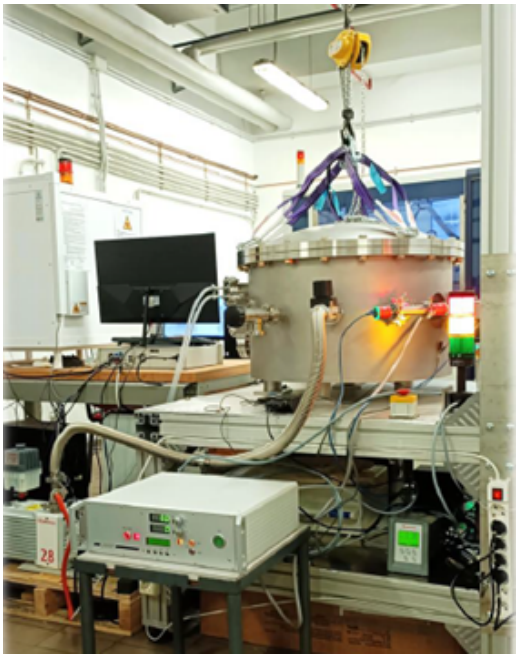

(a)

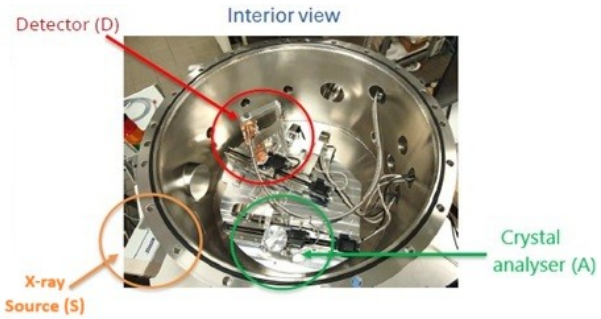

(b)

Figure 1: Overview of the LabXAS setup. (a) Photograph of the laboratory spectrometer developed at Politecnico di Milano. (b) Interior view indicating the positions of the X-ray source (S), crystal analyzer (A), and detector (D).

2.1. Rowland-Circle Configuration

The Rowland-circle condition links the source, analyzer, and detector positions so that rays satisfying the Bragg condition are focused onto the detector.[2] For a given reflection and Bragg angle, this focusing is achieved only when the geometry is consistent with the nominal Rowland radius; as a result, the measured line profile and its linewidth are highly sensitive to both alignment and radius detuning. In practice, small deviations in distance or angle can broaden the response and reduce the collected intensity, making the Rowland-radius setting a primary control parameter during commissioning.

This sensitivity is relevant for both analyzer geometries investigated in this work: the Johann-type spherically bent crystal analyzer (XRS) and the Johansson-type bent-crystal analyzer (Luxium). While both rely on the same Rowland-circle principle, their different geometrical implementations can lead to different focusing behavior and line-shape characteristics, which motivates the systematic radius-scan benchmarking and the quantitative comparison reported in the following sections. To validate the analyzers under controlled conditions, measurements were carried out at the ESRF ID26 beamline. This beamline uses a Rowland-circle spectrometer setup that is very similar to the LabXAS geometry and works in the same energy range. For this reason, ID26 is a convenient test platform to collect commissioning data before operating the analyzers in our laboratory. Figure 2 illustrates the Rowland-circle source–analyzer–detector geometry used in LabXAS.

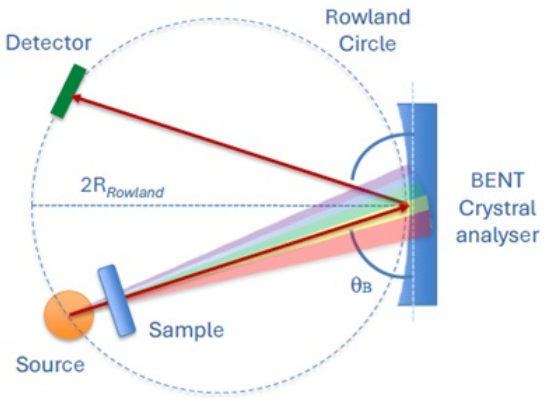

Figure 2: Table-top instrument in Johann geometry. The Bragg angle θ_B sets the selected photon energy, while the diffracted beam is focused onto the detector.

3. Methods

Two standard synchrotron scan were used:

- *Elastic energy scans:* the incident (monochromator) energy was scanned over a narrow window at fixed analyzer angle, and the detected signal originated from elastic scattering ($\Delta E \approx 0$), i.e. this window spans was about 6.3966–6.4124 kev.
- *Fluorescence rocking scans:* at fixed incident energy, the analyzer angle was scanned across the Bragg condition. When the angle matches the emission Bragg condition, the reflected in-

tensity is maximized and the detector spot is brightest. For consistency with the elastic-scan analysis, the measured intensity as a function of angle was also converted to an energy scale using Bragg's law.

3.1. Detector-image analysis and ROI selection

For each scan, two-dimensional detector frames were integrated within a fixed region of interest (ROI) to obtain a one-dimensional intensity profile. All intensities were normalized by the incident-beam monitor I_0 to compensate for beam-intensity fluctuations and enable comparisons across scans. The resulting profiles were fitted (split-Gaussian for Luxium and split pseudo-Voigt for the reference) to extract the FWHM as a direct measure of the energy resolution. A series of scans was recorded while varying the nominal Rowland radius to identify the minimum-FWHM condition, and we also evaluated reflectivity-related metrics and the detector footprint.

In addition to ROI-based spectral extraction, we estimated the beam footprint directly from the same detector frames. For each frame, we applied a simple intensity threshold inside the analysis ROI to obtain a binary mask of the illuminated region, removed small isolated pixels, and kept only the main spot. The footprint length and width were then computed from the mask size and converted from pixels to millimetres using the detector pixel size, providing a practical check of footprint stability across the scan.

4. Results

In the following, we report the resulting performance metrics (normalized by I_0) extracted from the ROI-integrated detector frames.

Luxium elastic scans: Figure 3 shows representative Luxium elastic energy scans (normalized by I_0) recorded at different nominal Rowland radii. The scan close to best focus exhibits the sharpest and most intense response, while off-focus conditions show a broader and smoother profile, consistent with increasing defocus. This asymmetric peak shape is an expected behavior for this configuration and is consistent with previous observations reported in earlier studies.[3]

To quantify the energy resolution, we selected the best-focus scan and fitted the peak profile with a split-Gaussian model (Fig. 4). The extracted FWHM was used as the energy-resolution metric. The same procedure was repeated for the other crystal under the same scan strategy and analysis workflow. By repeating the measurement across the radius series, the minimum-FWHM condition was identified at the optimum Rowland radius R_{opt}.

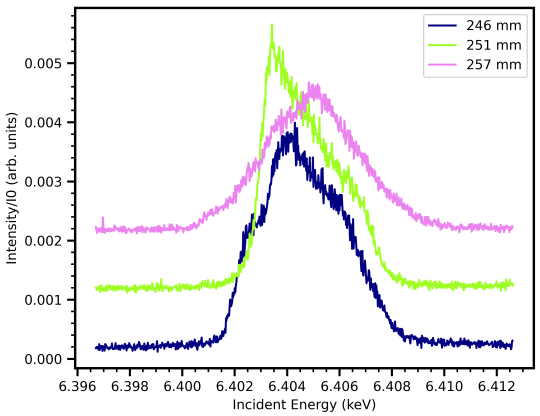

Figure 3: Representative Luxium elastic energy scans (normalized by I_0) acquired at three Rowland radii: $R = 246$ mm (blue), $R = 251$ mm (green, close to the optimum focusing condition), and $R = 257$ mm (purple). The optimum condition shows the sharpest and most intense response, while out-of-focus radii exhibit a broader, smoother lineshape consistent with increasing defocus.

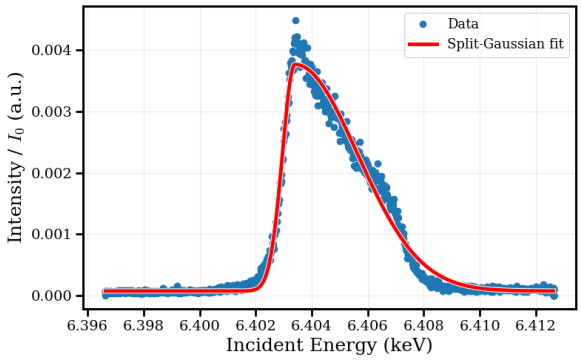

Figure 4: Best-fit line-shape representative Luxium elastic scan selected from Fig. 3. This fit curve is taken by using a split-Gaussian model.

4.1. Detector footprint behavior

Figure 5 shows representative Luxium detector footprints during the elastic scan at the optimum Rowland setting. The ROI is kept fixed, but the elongated spot shifts on the detector from frame to frame. The summed image over the full scan (Fig. 6) therefore covers a larger region (about ∼30 mm), while individual frames can appear shorter because only the subset of rays satisfying the Bragg condition at a given scan point contributes with strong intensity.
Overall, the accumulated footprint length (∼30 mm) is about half of the Luxium crystal length (60 mm) and is consistent with the footprint extent predicted by ray-tracing simulations [3].

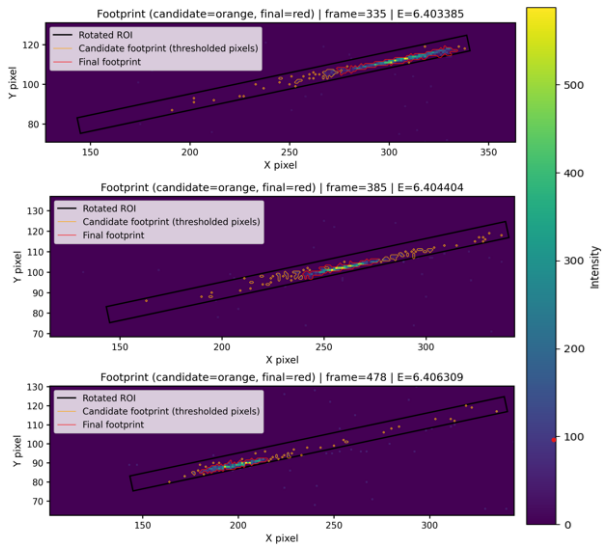

Figure 5: Zoomed detector-footprint images for Luxium elastic frames, showing the spot position and shape within the fixed rotated ROI across the scan.

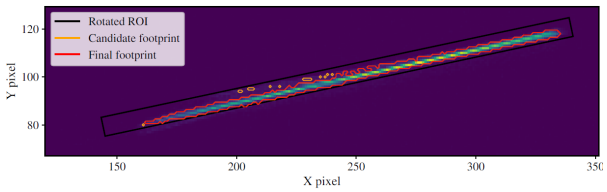

Figure 6: Summed detector image obtained by accumulating all frames of the scan. The resulting map highlights the overall footprint extent (about 30 mm).

4.2. Reference analyzer summary and quantitative tables

The XRS analyzer is used as a reference benchmark. For this analyzer, the key results are summarized in Tables 1 , 2 and 3 .

Metric	Luxium	XRS
R_{opt} (mm)	251	253
$\mathrm{FWHM}_{\mathrm{min}}$ (eV)	3.05	0.91

Table 1: R_{opt} and elastic $\mathrm{FWHM}_{\mathrm{min}}$ for Luxium (CBCA) and XRS (SBCA).

Frame number	335	385	478
L_{fp} (mm)	10.58	6.64	6.31
W_{fp} (mm)	1.03	0.93	0.92
E_{fr} (keV)	6.403	6.404	6.406

Table 2: Luxium footprint metrics for three representative frames. L_{fp} and W_{fp} denote the footprint length and width (mm) in the ROI-aligned coordinate system (along x' and y', respectively). E_{fr} is the monochromator energy associated with each frame (keV).

Frame number	377	385	400
L_{fp} (mm)	12.55	13.41	13.41
W_{fp} (mm)	1.54	1.54	1.54
E_{fr} (keV)	6.3992	6.3993	6.3996

Table 3: XRS footprint metrics and corresponding energies for three representative frames.

4.3. Fluorescence rocking scans on different emission lines: Ge(220) vs Ge(440)

In the fluorescence rocking-scan measurements, different emission lines were investigated at different photon energies. Specifically, the Luxium analyzer was tested in the tender-energy configuration using the Pd Lβ line with the Ge(220) reflection (TEXS), and in the hard X-ray configuration using the Fe Kα line with the Ge(440) reflection. The table below summarizes the key figures of merit extracted for these two cases. To separate the spectrometer contribution from the

intrinsic width of the fluorescence line, we corrected the measured linewidth using a quadratic deconvolution. Assuming that the experimental profile can be approximated by the convolution of the instrumental response with the natural emission line profile, the FWHM contributions add in quadrature:

$$\Delta E_{\mathrm{exp}}^2 \approx \Delta E_{\mathrm{instr}}^2 + \Delta E_{\mathrm{nat}}^2, \quad (1)$$

so that the instrumental linewidth is obtained as

$$\Delta E_{\mathrm{instr}} = \sqrt{\Delta E_{\mathrm{exp}}^2 - \Delta E_{\mathrm{nat}}^2}. \quad (2)$$

Here ΔE_{nat} is the intrinsic (natural) linewidth of the selected fluorescence transition, taken from the compilation of K$\alpha_{1,2}$ and K$\beta_{1,3}$ emission lines by Hölzer *et al.* [4]. Because the two rocking-scan experiments probe emission lines at different photon energies—Pd Lβ in the tender-energy range ($E \approx 3.3$ keV) and Fe Kα in the hard X-ray range ($E \approx 6.40$ keV)—their experimental linewidths are not directly comparable without correcting for the intrinsic line broadening. The main figures of merit for these two cases (Pd Lβ/Ge(220) in TEXS and Fe Kα/Ge(440) in hard X-ray) are summarized in Table 4.

Metric	**Ge(220)**	**Ge(440)**
FWHM ΔE_{exp} (eV)	5.12	3.48
$\Delta E_{\mathrm{instr}}$ (eV)	4.60	1.50
L_{fp} (mm)	32.36	32.87
W_{fp} (mm)	1.46	1.05

Table 4: Summary of fluorescence rocking-scan figures of merit for Luxium measured on two emission lines at different energies: Pd Lβ in the TEXS configuration using Ge(220), and Fe Kα in the hard X-ray configuration using Ge(440). Here L_{fp} and W_{fp} denote the footprint length and width, respectively.

4.4. Reflectivity

A reflectivity proxy was defined from the ROI-integrated detector signal and the incident monitor:

$$R(E) = \frac{I_{\mathrm{det}}(E)}{I_0(E)}. \quad (3)$$

To compare configurations with different acceptance (illuminated area on the analyzer), we also report an area-normalized reflectivity:

$$R_{\mathrm{norm}}(E) = \frac{I_{\mathrm{det}}(E)}{I_0(E)\,A}, \quad (4)$$

where A is the physical surface area of the analyzer crystal. For the CBCA, we use $A_{\mathrm{Lux}} = 60 \times 15\ \mathrm{mm}^2 = 900\ \mathrm{mm}^2$, whereas for the XRS SBCA we use $A_{\mathrm{XRS}} = \pi(50\ \mathrm{mm})^2 \approx 7850\ \mathrm{mm}^2$. Using the integrated area of $R_{\mathrm{norm}}(E)$, we obtain the area-based comparison factor

$$\eta_{\mathrm{area}} = \frac{S_{\mathrm{norm}}^{\mathrm{CBCA}}}{S_{\mathrm{norm}}^{\mathrm{SBCA}}} = 4.76. \quad (5)$$

5. Conclusions

This work reports the commissioning of a Ge(nn0) bent-crystal analyzer for LabXAS at Politecnico di Milano. An ROI-based workflow reduces 2D detector images to consistent 1D curves for elastic and fluorescence scans, enabling reliable extraction of the FWHM (energy resolution), footprint metrics, and normalized reflectivity indicators. The analysis provides a clear performance map versus spectrometer configuration and identifies the optimum Rowland setting that delivers the best resolution for the Luxium analyzer. Asymmetric elastic line shapes were handled with an asymmetric fit model to ensure stable linewidth trends across scans, and fluorescence widths were corrected to isolate the instrumental contribution from the intrinsic emission-line broadening.

The next step is to transfer the commissioned analyzer and the validated alignment/analysis protocol to the in-house LabXAS instrument, where the identified optimum setting can be used as a starting point to achieve the best resolution in the laboratory and to enable routine XAS measurements without relying on synchrotron beamtime.

6. Acknowledgements

I sincerely thank my supervisor, Prof. Marco Moretti, for his guidance, Dr. Roberto Sant for his continuous feedback and practical support during the commissioning and analysis, and Prof. Giacomo Ghiringhelli for his encouragement. I gratefully acknowledge the PoliMiX group and all colleagues who contributed through discussions, technical help, and day-to-day collaboration.

References

[1] Diego Gianolio. How to start an xas experiment. In Jeroen A. van Bokhoven and Carlo Lamberti, editors, *X-Ray Absorption and X-Ray Emission Spectroscopy: Theory and Applications*, pages 99–124. John Wiley & Sons, Ltd, 2016. doi: 10.1002/9781118844243.ch5.

[2] A.-P. Honkanen et al. Improving the energy resolution of bent crystal x-ray spectrometers. *Journal of Synchrotron Radiation*, 2014. Open access via PMC.

[3] Piero Florio. Performance analysis and simulations of a laboratory x-ray absorption spectrometer. Master's thesis, Politecnico di Milano, 2022. Chapters 6–7 (intrinsic contribution, dynamical diffraction in bent crystals).

[4] G. Hölzer, M. Fritsch, M. Deutsch, J. Härtwig, and E. Förster. K$\alpha_{1,2}$ and k$\beta_{1,3}$ x-ray emission lines of the 3d transition metals. *Physical Review A*, 56(6):4554–4568, 1997. doi: 10.1103/PhysRevA.56.4554.